Electronic Supplementary Material (ESI) for Polymer Chemistry.
This journal is © The Royal Society of Chemistry 2018

Supporting Information

Installing Lactone Chain Termini During Photoinduced Polymerization

Andrea Lauer,[a,b,c,‡] Jan Steinkoenig,[a,b,c,‡] Philipp Jöckle,[a,b,c,e] Anne-Marie Kelterer,[d,*] Andreas N. Unterreiner,[e,*] and Christopher Barner-Kowollik[a,b,c,*]

[a] School of Chemistry, Physics and Mechanical Engineering, Queensland University of Technology (QUT), 2 George Street, QLD 4000, Brisbane, Australia, christopher.barnerkowollik@qut.edu.au

[b] Macromolecular Architectures, Institut für Technische Chemie und Polymerchemie, Karlsruhe Institute of Technology (KIT), Engesserstr. 18, 76131 Karlsruhe, Germany, christopher.barner-kowollik@kit.edu

[c] Institut für Biologische Grenzflächen (IBG), Karlsruhe Institute of Technology (KIT), Herrmann-von-Helmholtz-Platz 1, 76344 Eggenstein-Leopoldshafen, Germany

[d] Institute of Physical and Theoretical Chemistry, NAWI Graz, Graz University of Technology, Stremayrgasse 9, 8010 Graz, Austria, kelterer@tugraz.at

[e] Molekulare Physikalische Chemie, Institut für Physikalische Chemie, Karlsruhe Institute of Technology (KIT), Fritz-Haber-Weg 2, 76131 Karlsruhe, Germany, andreas.unterreiner@kit.edu

[‡] These authors contributed equally

1. Materials

2-Hydroxy-4'-(2-hydroxyethoxy)-2-methylpropiophenone (Irgacure 2959) and 2-Methyl-4'-(methylthio)-2-morpholinopropiophenone (Irgacure 907) were kindly provided by BASF and used as purchased. Methyl methacrylate (MMA, Sigma-Aldrich, 99%, stabilized), ethyl methacrylate (EMA, TCI, 99%, stabilized), *n*-propyl methacrylate (*n*PMA, Sigma-Aldrich, 97%, stabilized), iso-propyl methacrylate (*i*PMA, TCI, 98%, stabilized), *n*-butyl methacrylate (*n*BMA, Sigma-Aldrich, 99%, stabilized), tert-butyl methacrylate (*t*BMA, Sigma-Aldrich, 98%, stabilized), benzyl methacrylate (BnMA, TCI, 98%, stabilized), dimethyl amino-ethyl methacrylate (DMAEMA, TCI, 98.5%, stabilized), were deinhibated by passing through a column of activated basic alumina (Sigma-Aldrich). Sodium iodide (Sigma-Aldrich, 99%), trifluoracetate (Sigma-Aldrich, 99%), tetrahydrofuran (THF, Scharlau, multisolvent GPC grade, 250 ppm BHT), and methanol (Roth, HPLC ultra gradient grade) for SEC-ESI-MS and direct infusion ESI-MS measurements were employed as received. For pulsed-laser polymerization we used crimp photo glass vials (Lab Logistic Group GmbH (Art. Nr. 4-008202)) as well crimped quartz glass vials ilmasil PS (Qsil GmbH Quarzschmelze Ilmenau (Art.Nr. G540PS000000176)).

2. Instrumental Methods

2.1 Pulsed-Laser Polymerization (PLP)

The PLP samples for the energy- and temperature-dependent study were all prepared with a concentration of $c_{\text{Photoinitiator}} = 5 \cdot 10^{-3}$ mol·L^{-1} in monomer (sample volume ~ 0.4 mL, crimped photo glass vials (Lab Logistic Group GmbH, Art. Nr. 4-008202)) and freed from oxygen by purging with nitrogen for 2 minutes. Subsequently, the samples were individually placed into the sample holder, which was held at a constant temperature by a thermostat (model: 1196D, VWR, Darmstadt, Germany). Polymerizations were carried out by an excimer laser system (Coherent XS-500, XeF, 351 nm, frequency variable from 1-500 Hz). The temperature-dependent polymerizations were performed at a laser energy of 0.35 mJ/pulse (custom-build metal filter was implemented to reduce the laser energy). After the polymerization, the remaining monomer

was evaporated and the polymer was used without further purification for SEC-ESI-MS measurements. Refer to **Table S13-S14** for the applied irradiation parameters.

2.2 Wavelength-Variable Pulsed-Laser Polymerization (PLP)

The PLP samples for the wavelenght- and monomer-dependent (λ = 351 nm) study were all prepared with a concentration of $c_{Photoinitiator}$ = $5 \cdot 10^{-3}$ mol·L^{-1} in monomer (sample volume close to 0.4 mL, crimped photo glass vials (Lab Logistic Group GmbH, Art. Nr. 4-008202) as well crimped quartz glass vials ilmasil PS (Qsil GmbH Quarzschmelze Ilmenau, Art.Nr. G540PS000000176)) and freed from oxygen by purging with nitrogen for 2 minutes. Subsequently, the samples were individually placed into the sample holder and irradiated at ambient temperature. The polymerizations were carried out by a tunable laser system (SpitLight 600 OPO, λ = 270-650 nm) with low laser energy of 0.35 mJ/pulse. Tunable UV/Vis laser light was generated by an Innolas Tunable Laser System SpitLight 600 OPO. An optical parametric oscillator (OPO) was pumped with a diode pumped Nd:YAG laser (repetition rate 100 Hz). The energy output of the laser was regulated by an attenuator (polarizer). As shown in Scheme S1, the laser beam is redirected by a prism and enters the sample in a custom-made sample holder from below. The sample holder consists of a metal block with a vertical cylindrical hole (0.71 cm diameter), fixing the crimped glass vials during experiments. The energy of the incident laser pulses was measured via an Energy Max PC power meter (Coherent). Subsequently, the polymers were dried under air and used without further purification for SEC-ESI-MS measurements. Refer to **Table S11-S12** for the applied irradiation parameters.

Scheme S1. Experimental Setup for the Measurement of the Laser Energy

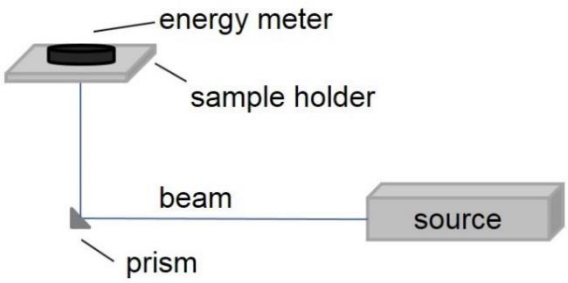

Calibration Procedure for Constant Photon Count:[S1]

The transmittance of the crimped photo glass vials that were used for photoreactions with the tunable laser system was determined experimentally using the tunable laser setup. The transmittance of the crimped quartz glass vials were used as received from the company Qsil GmbH (refer to **Table S1** and **Figure S2**). Measurement of the energy of laser pulses at a constant energy output was carried out directly above the sample holder, first without a crimped photo glass vial in the sample holder and subsequently with an empty crimped photo glass vial in the sample holder. The top part of the crimped photo glass vial was removed for these measurements (**Figure S1**). Thus, only the absorbance of the bottom of the crimped photo glass vial is detected. The described procedure was performed for three individual crimped photo glass vials to account for variability between the vials. The obtained averaged values are listed in **Table S1**.

Figure S1. Left: vial after removal of the top part; right: crimped photo glass vial.

Table S1. Transmittance of Crimped Photo Glass Vials and Crimped Quartz Glass Vials

	Crimped Photo Glass Vials		Crimped Quartz Glass Vials
λ / nm	**mean transmittance / %**	**mean deviation / %**	**transmittance / %**
270	0	0	91.8
275	0	0	91.8
280	0	0	91.9
285	13.4	0.2	92.0
290	19.7	0.6	92.1
295	30.3	0.5	92.1
300	37.7	1.0	92.2
305	45.6	0.5	92.2
310	47.5	1.0	92.3
315	51.1	0.6	92.3
320	56.3	1.2	92.3
325	58.9	0.8	92.4
330	61.0	0.9	92.4
335	62.9	0.9	92.4
340	60.4	0.9	92.4
345	64.5	1.6	92.4
350	60.4	1.1	92.5
355	62.1	0.9	92.5
360	65.1	0.3	92.5
370	65.9	1.2	92.5
380	66.3	1.2	92.5
390	70.8	0.4	92.5
400	66.9	0.9	92.5
410	68.0	1.9	-
430	75.3	0.6	-
450	76.6	0.8	-
470	77.6	0.5	-
490	79.1	0.5	-

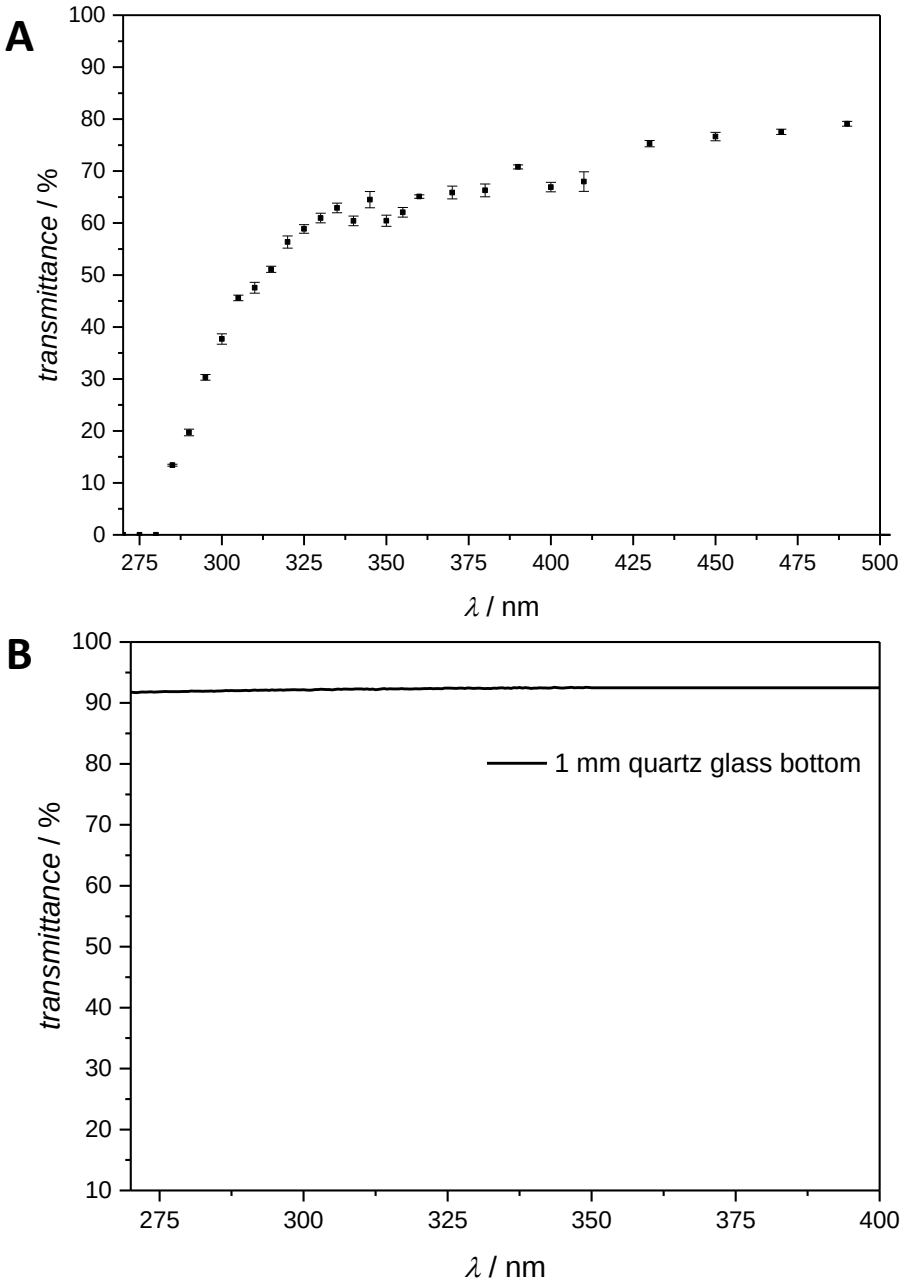

Figure S2. Transmittance of crimped photo glass vials (A) and crimped quartz glass vials (B) dependent on irradiation wavelength.

For all irradiation wavelengths 'target energy' was calculated. The target energy per pulse (E^0) was defined as the measured energy in case of an empty sample holder. For each irradiation experiment the attenuator position, defined and controlled by the measurement of E^0, enables

irradiation of each sample solution with a defined number of photons. The target energy per pulse E^0 was calculated according to eq. S1 with the wavelength λ, the number of pulses $\boldsymbol{k}$, the transmittance of the glass vial at the respective wavelength $\boldsymbol{T_\lambda}$ and the desired total photon count $\boldsymbol{n_{h\nu}}$.

$$E^0 = \frac{n_{h\nu} * h * c}{k * T_\lambda * \lambda} \qquad \text{(eq. S1)}$$

Thus, the number of photons penetrating each sample solution is equal.

2.3 Size Exclusion Chromatography - Electrospray Ionization - Mass Spectrometry (SEC-ESI-MS)

Spectra were recorded on a Q Exactive (Orbitrap) mass spectrometer (Thermo Fisher Scientific, San Jose, CA, USA) equipped with an HESI II probe. The instrument was calibrated in the m/z range 74-1822 using premixed calibration solutions (Thermo Scientific). A constant spray voltage of 4.6 kV, a dimensionless sheath gas of 8, and a dimensionless auxiliary gas flow rate of 2 were applied. The capillary temperature and the S-lens RF level were set to 320 °C and 62.0, respectively. The Q Exactive was coupled to an UltiMate 3000 UHPLC System (Dionex, Sunnyvale, CA, USA) consisting of a pump (LPG 3400SD), autosampler (WPS 3000TSL), and a thermostated column department (TCC 3000SD). Separation was performed on two mixed bed size exclusion chromatography columns (Polymer Laboratories, Mesopore 250 × 4.6 mm, particle diameter 3 µm) with precolumn (Mesopore 50 × 4.6 mm) operating at 30 °C. THF at a flow rate of 0.30 mL·min^{-1} was used as eluent. The mass spectrometer was coupled to the column in parallel to a RI-detector (RefractoMax520, ERC, Japan) in a setup described earlier. 0.27 mL·min^{-1} of the eluent were directed through the RI-detector and 30 µL·min^{-1} infused into the electrospray source after postcolumn addition of a 100 µM solution of sodium iodide in methanol at 20 µL·min^{-1} by a micro-flow HPLC syringe pump (Teledyne ISCO, Model 100DM). A 100 µL aliquot of a polymer solution with a concentration of 2 mg·mL^{-1} was injected into the HPLC system.

2.4 Electrospray Ionization - Mass Spectrometry (ESI-MS)

Mass spectra were recorded on a Q Exactive (Orbitrap) mass spectrometer (Thermo Fisher Scientific, San Jose, CA, USA) equipped with an HESI II probe. The instrument was calibrated in the m/z range 74-1822 using premixed calibration solutions (Thermo Scientific). A constant spray voltage of 4.7 kV and a dimensionless sheath gas of 5 were applied. The capillary temperature and the S-lens RF level were set to 320 °C and 62.0, respectively. The samples were dissolved with a concentration of 0.05 $mg \cdot mL^{-1}$ in a mixture of THF and MeOH (3:2) containing 100 µmol of sodium trifluoroacetate and infused with a flow of 5 $\mu L \cdot min^{-1}$.

2.5 Nuclear Magnetic Resonance (NMR) measurements

^{13}C NMR spectra of the polymers were recorded on a Bruker AM 400 spectrometer (100 MHz). All samples were dissolved in $CDCl_3$ and measured with 5120 scans.

2.6 DFT Calculations

The polymer model used for the calculations of the energetics and barriers includes two monomer units of the propyl (R3) and butyl (R4) substituents, respectively. Optimizations of the geometries were carried out by Density Functional Theory (DFT) using the M06-2X functional.[S2] Grimme's dispersion correction[S3] with Becke-Johnson damping[S4] (D3BJ) was applied to account the dispersion interaction of the alkyl chains. Harmonic model frequency calculations were performed to characterize the geometries as minima at the potential energy surface and to receive the Gibbs free energies at room temperature (298 K). The aug-cc-pVDZ basis set was used for optimizations and frequency calculations. To improve the energetics, the larger aug-cc-pVTZ basis set[S5,6] was used for single point energies and for the correction of Gibbs free energies by adding the electronic energy difference of large and small basis set. To model the monomer surrounding, the IEF-PCM solvation model[S7] in DMSO was selected. The program Gaussian09[S8] was used throughout the study.

3. Evaluation

3.1 High resolution SEC-ESI-MS

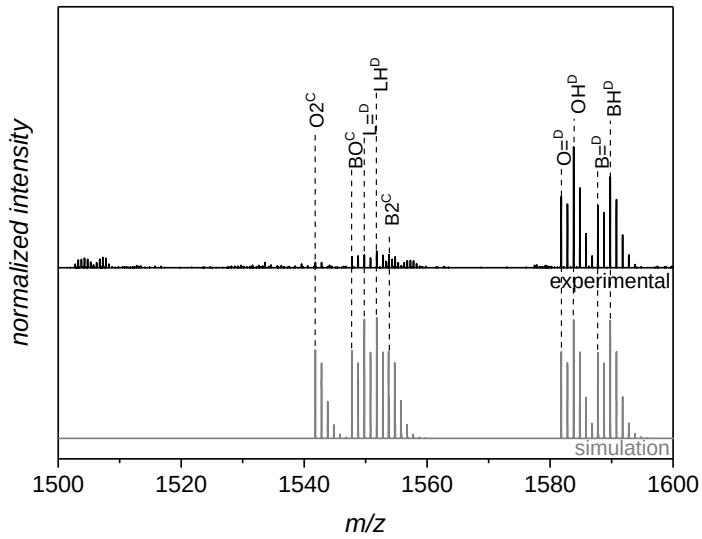

Figure S3. High resolution SEC-ESI mass spectra of the p(MMA) initiated by Irgacure 2959, synthesized at low laser energies (0.35 mJ/pulse, 100 Hz, 351 nm, 18°C, black spectrum), and the associated isotopic pattern simulation (gray spectrum).

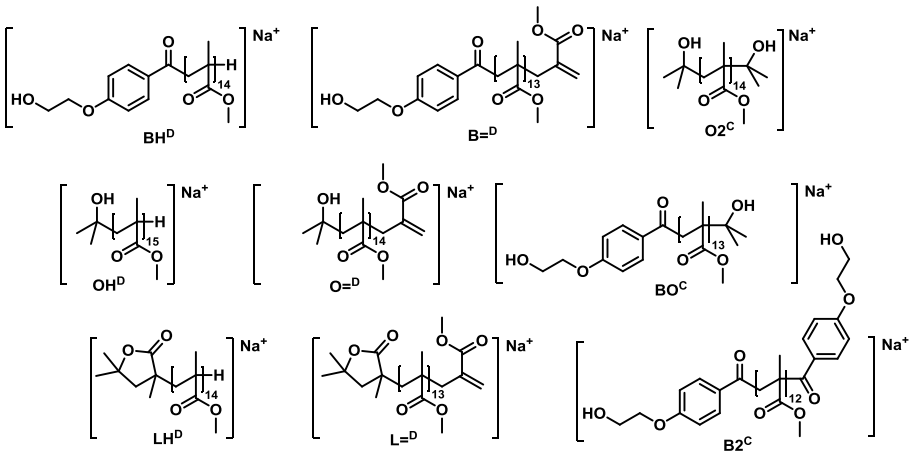

Scheme S2. Disproportionation and combination products of p(MMA) initiated by Irgacure 2959, at low laser energies (0.35 mJ/pulse, 100 Hz, 351 nm, 18 °C), as detected by SEC-ESI-MS.

Table S2. Overview of the assigned signals of p(MMA) synthesized at low laser energies (351 nm, 0.35 mJ/pulse, 100 Hz), as detected by SEC-ESI-MS with a resolution of 50000.

species	ionization	$(m/z)^{theo}$	$(m/z)^{exp}$	$\Delta(m/z)$
BH^D	Na^+	1589.7862	1589.7794	0.0068
$B{=}^D$	Na^+	1587.7706	1587.7671	0.0035
OH^D	Na^+	1583.8332	1583.8294	0.0038
$O{=}^D$	Na^+	1581.8175	1581.8135	0.0040
LH^D	Na^+	1551.8070	1551.8022	0.0048
$L{=}^D$	Na^+	1549.7913	1549.7900	0.0013
$B2^C$	Na^+	1553.7287	1553.7274	0.0013
$O2^C$	Na^+	1541.8226	1541.8224	0.0002
BO^C	Na^+	1547.7757	1547.7774	0.0017

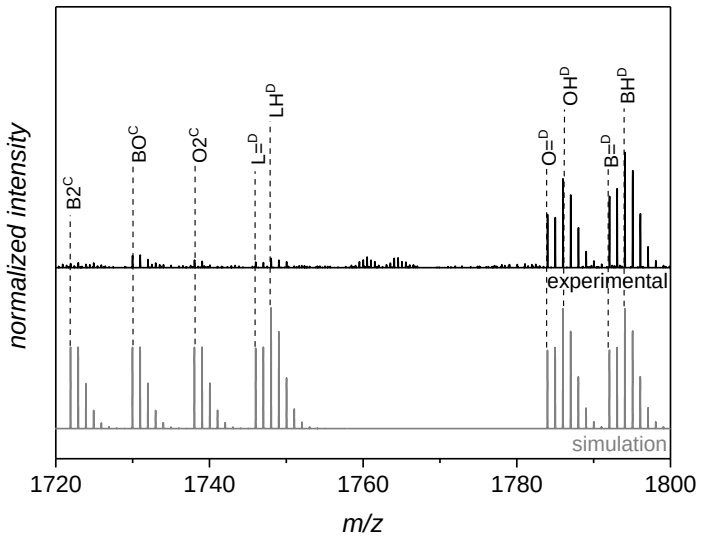

Figure S4. High resolution SEC-ESI mass spectra of p(EMA) initiated by Irgacure 2959, synthesized at low laser energies (0.35 mJ/pulse, 100 Hz, 351 nm, black spectrum), and the associated isotopic pattern simulation (gray spectrum).

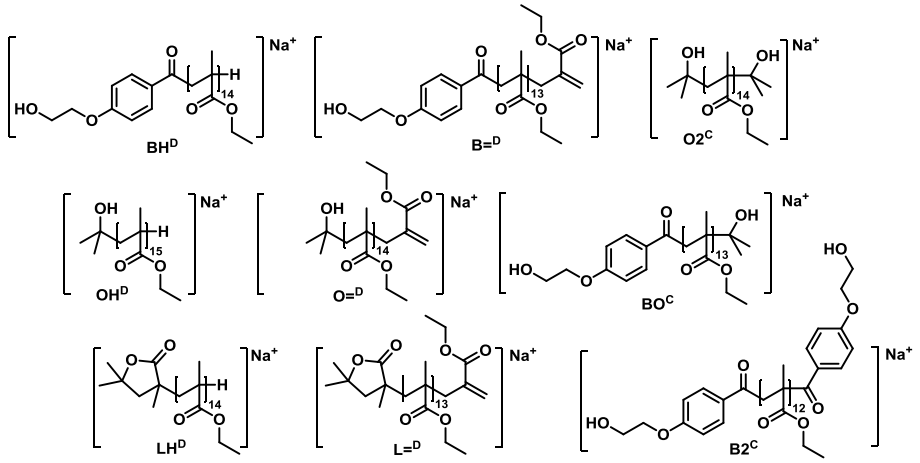

Scheme S3. Disproportionation and combination products of p(EMA) initiated by Irgacure 2959, at low laser energies (0.35 mJ/pulse, 100 Hz, 351 nm), as detected by SEC-ESI-MS.

Table S3. Overview of the assigned signals of p(EMA) synthesized at low laser energies (351 nm, 0.35 mJ/pulse, 100 Hz), as detected by SEC-ESI-MS with a resolution of 50000.

species	ionization	$(m/z)^{theo}$	$(m/z)^{exp}$	$\Delta(m/z)$
BH^D	Na^+	1786.0053	1786.0138	0.0085
B=^{D}	Na^+	1783.9897	1784.0021	0.0124
OH^D	Na^+	1794.0679	1794.0765	0.0086
O=^{D}	Na^+	1792.0523	1792.0602	0.0079
LH^D	Na^+	1748.0261	1748.0363	0.0102
L=^{D}	Na^+	1746.0104	1746.0193	0.0089
B2^C	Na^+	1721.9165	1721.9320	0.0155
O2^C	Na^+	1738.0417	1738.0546	0.0129
BO^C	Na^+	1729.9791	1729.9907	0.0116

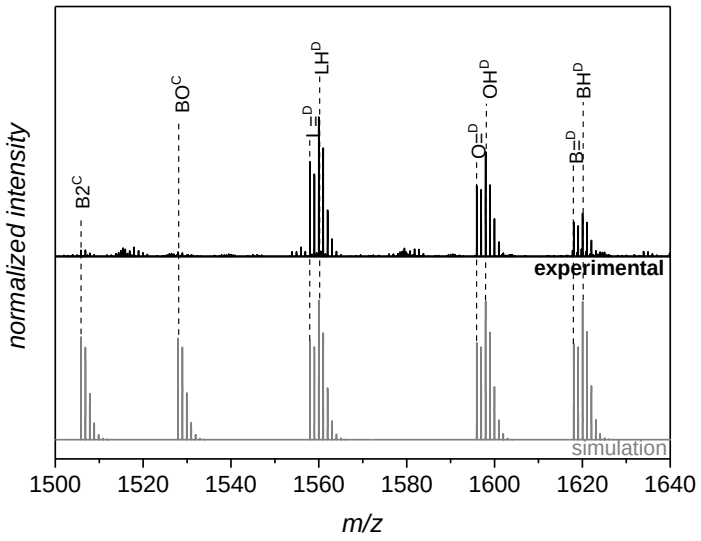

Figure S5. High resolution SEC-ESI mass spectra of p(*n*PMA) initiated by Irgacure 2959, synthesized at low laser energies (0.35 mJ/pulse, 100 Hz, 351 nm, black spectrum), and the associated isotopic pattern simulation (gray spectrum).

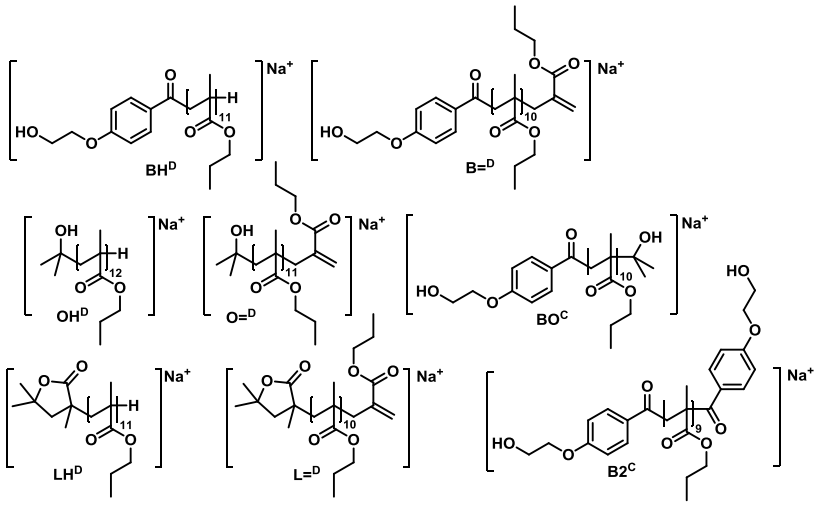

Scheme S4. Disproportionation and combination products of p(*n*PMA) initiated by Irgacure 2959, at low laser energies (0.35 mJ/pulse, 100 Hz, 351 nm, 18 °C), as detected by SEC-ESI-MS.

Table S4. Overview of the assigned signals of p(*n*PMA) synthesized at low laser energies (351 nm, 0.35 mJ/pulse, 100 Hz), as detected by SEC-ESI-MS with a resolution of 50000.

species	ionization	$(m/z)^{theo}$	$(m/z)^{exp}$	$\Delta(m/z)$
BH^D	Na^+	1597.9732	1597.9718	0.0014
$B{=}^D$	Na^+	1595.9576	1595.9593	0.0017
OH^D	Na^+	1620.0515	1620.0460	0.0055
$O{=}^D$	Na^+	1618.0358	1618.0379	0.0021
LH^D	Na^+	1559.9940	1559.9948	0.0008
$L{=}^D$	Na^+	1557.9783	1557.9806	0.0023
$B2^C$	Na^+	1505.8531	1505.8507	0.0025
BO^C	Na^+	1527.9314	1527.9335	0.0021

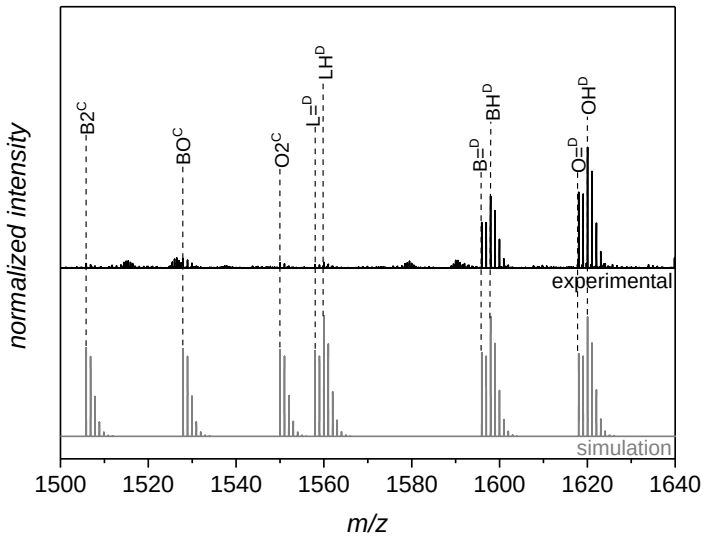

Figure S6. High resolution SEC-ESI mass spectra of p(*i*PMA) initiated by Irgacure 2959, synthesized at low laser energies (0.35 mJ/pulse, 100 Hz, 351 nm, black spectrum), and the associated isotopic pattern simulation (gray spectrum).

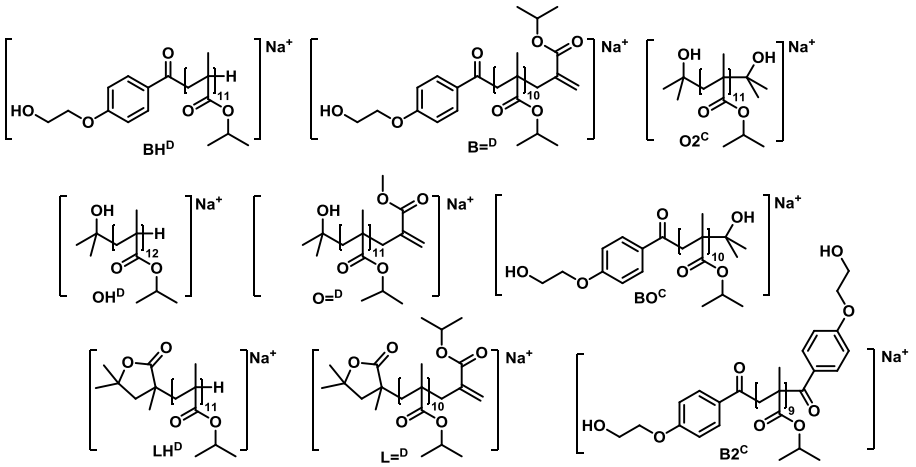

Scheme S5. Disproportionation and combination products of p(*i*PMA) initiated by Irgacure 2959, at low laser energies (0.35 mJ/pulse, 100 Hz, 351 nm, 18 °C), as detected by SEC-ESI-MS.

Table S5. Overview of the assigned signals of p(*i*PMA) synthesized at low laser energies (351 nm, 0.35 mJ/pulse, 100 Hz), as detected by SEC-ESI-MS with a resolution of 50000.

species	ionization	$(m/z)^{theo}$	$(m/z)^{exp}$	$\Delta(m/z)$
BH^{D}	Na^+	1597.9732	1597.9677	0.0055
B=^{D}	Na^+	1595.9576	1595.9551	0.0025
OH^{D}	Na^+	1620.0515	1620.0493	0.0022
O=^{D}	Na^+	1618.0358	1618.0333	0.0025
LH^{D}	Na^+	1559.9940	1559.9902	0.0038
L=^{D}	Na^+	1557.9783	1557.9735	0.0048
B2^{C}	Na^+	1505.8531	1505.8550	0.0019
O2^{C}	Na^+	1550.0096	1550.0101	0.0005
BO^{C}	Na^+	1527.9314	1527.9298	0.0016

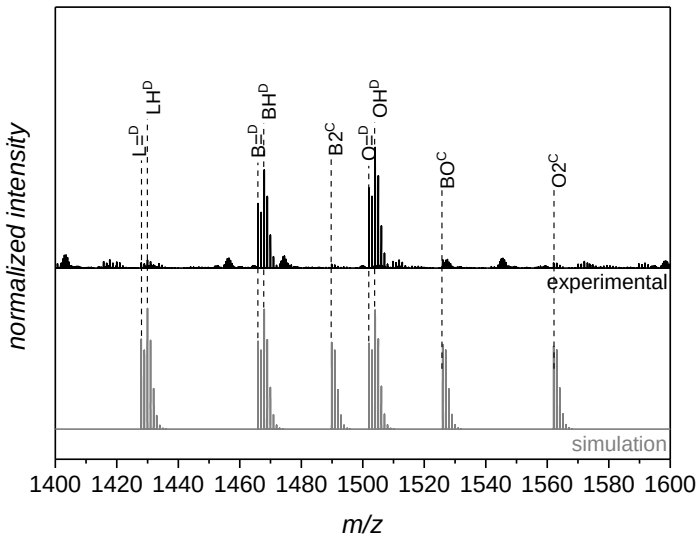

Figure S7. High resolution SEC-ESI mass spectra of p(*n*BMA) initiated by Irgacure 2959, synthesized at low laser energies (0.35 mJ/pulse, 100 Hz, 351 nm, black spectrum), and the associated isotopic pattern simulation (gray spectrum).

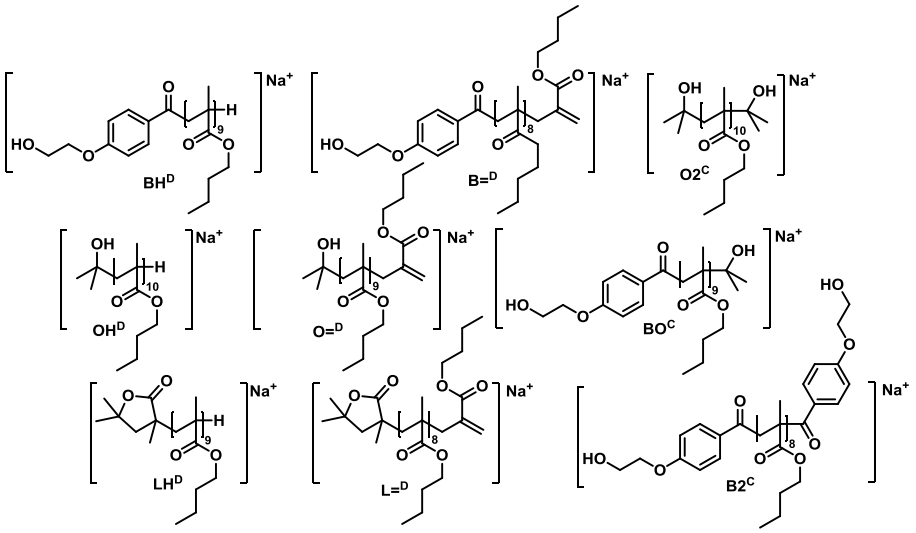

Scheme S6. Disproportionation and combination products of p(*n*BMA) initiated by Irgacure 2959, at low laser energies (0.35 mJ/pulse, 100 Hz, 351 nm), as detected by SEC-ESI-MS.

Table S6. Overview of the assigned signals of p(*n*BMA) synthesized at low laser energies (351 nm, 0.35 mJ/pulse, 100 Hz), as detected by SEC-ESI-MS with a resolution of 50000.

species	ionization	$(m/z)^{theo}$	$(m/z)^{exp}$	$\Delta(m/z)$
BH^D	Na^+	1467.9466	1467.9435	0.0031
$B{=}^D$	Na^+	1465.9310	1465.9319	0.0009
OH^D	Na^+	1504.0405	1504.0346	0.0059
$O{=}^D$	Na^+	1502.0249	1502.0243	0.0006
LH^D	Na^+	1429.9674	1429.9640	0.0034
$L{=}^D$	Na^+	1427.9517	1427.9531	0.0014
$B2^C$	Na^+	1489.8946	1489.8968	0.0022
$O2^C$	Na^+	1562.0824	1562.0832	0.0008
BO^C	Na^+	1525.9885	1525.9855	0.0030

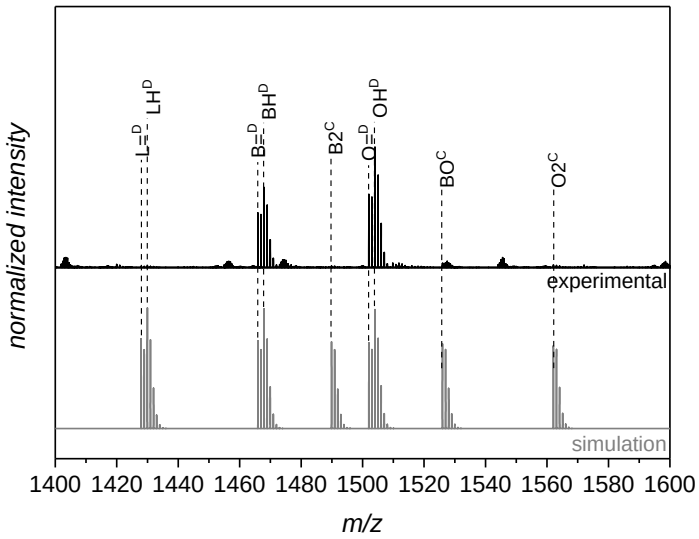

Figure S8. High resolution SEC-ESI mass spectra of p(*t*BMA) initiated by Irgacure 2959, synthesized at low laser energies (0.35 mJ/pulse, 100 Hz, 351 nm, black spectrum), and the associated isotopic pattern simulation (gray spectrum).

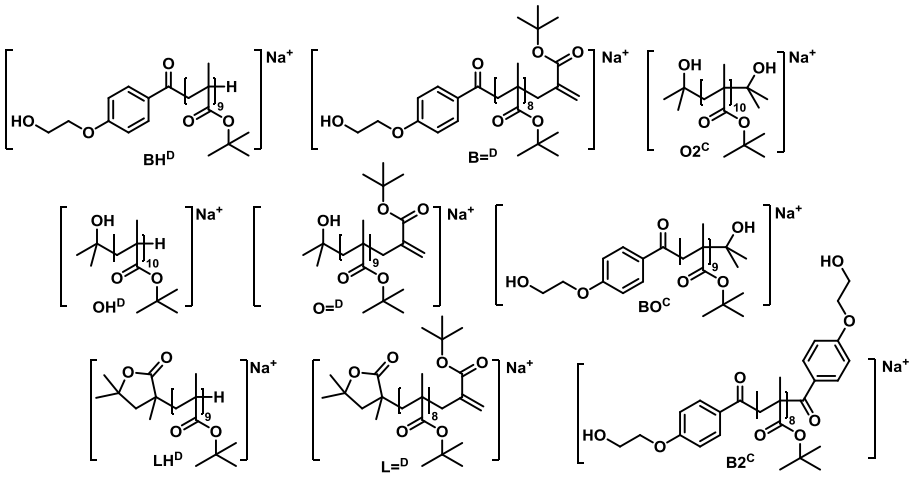

Scheme S7. Disproportionation and combination products of p(*t*BMA) initiated by Irgacure 2959, at low laser energies (0.35 mJ/pulse, 100 Hz, 351 nm), as detected by SEC-ESI-MS.

Table S7. Overview of the assigned signals of p(*t*BMA) synthesized at low laser energies (351 nm, 0.35 mJ/pulse, 100 Hz), as detected by SEC-ESI-MS with a resolution of 50000.

species	ionization	$(m/z)^{theo}$	$(m/z)^{exp}$	$\Delta(m/z)$
BH^D	Na^+	1467.9466	1467.9461	0.0005
B=^{D}	Na^+	1465.9310	1465.9279	0.0031
OH^D	Na^+	1504.0405	1504.0373	0.0032
O=^{D}	Na^+	1502.0249	1502.0201	0.0048
LH^D	Na^+	1429.9674	1429.9665	0.0009
L=^{D}	Na^+	1427.9517	1427.9493	0.0024
B2^C	Na^+	1489.8946	1489.8927	0.0019
O2^C	Na^+	1562.0824	1562.0787	0.0037
BO^C	Na^+	1525.9885	1525.9883	0.0002

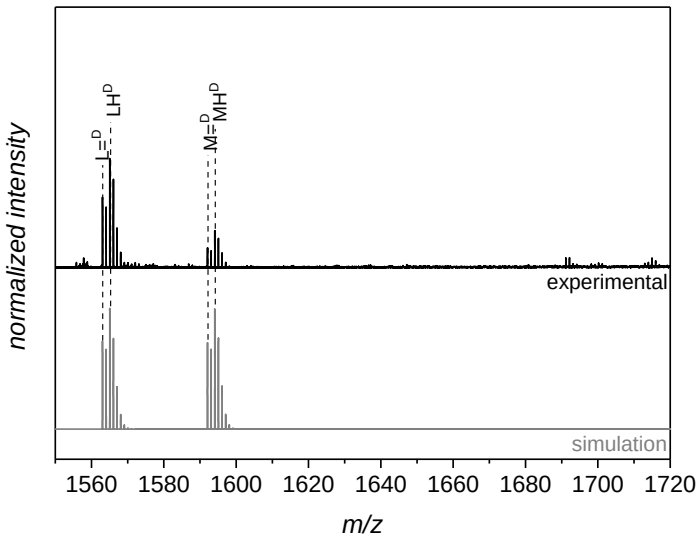

Figure S9. High resolution SEC-ESI mass spectra of p(DMAEMA) initiated by Irgacure 2959, synthesized at low laser energies (0.35 mJ/pulse, 100 Hz, 351 nm, black spectrum), and the associated isotopic pattern simulation (gray spectrum).

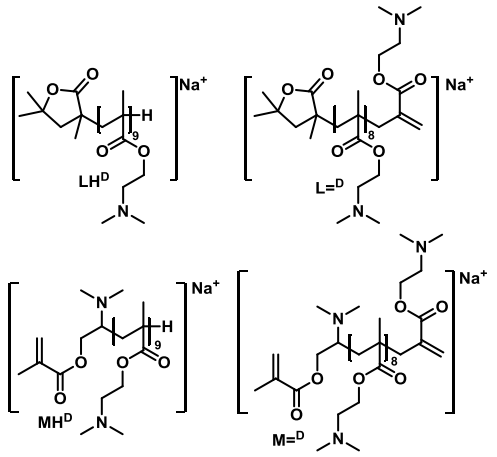

Scheme S8. Disproportionation and combination products of p(DMAEMA) initiated by Irgacure 2959, at low laser energies (0.35 mJ/pulse, 100 Hz, 351 nm), as detected by SEC-ESI-MS.

Table S8. Overview of the assigned signals of p(DMAEMA) synthesized at low laser energies (351 nm, 0.35 mJ/pulse, 100 Hz), as detected by SEC-ESI-MS with a resolution of 50000.

species	ionization	$(m/z)^{theo}$	$(m/z)^{exp}$	$\Delta(m/z)$
BH^D	Na^+	1565.0655	1565.0603	0.0052
$B{=}^D$	Na^+	1563.0498	1563.0510	0.0012
MH^D	Na^+	1594.0920	1594.0923	0.0003
$M{=}^D$	Na^+	1592.0764	1592.0720	0.0044

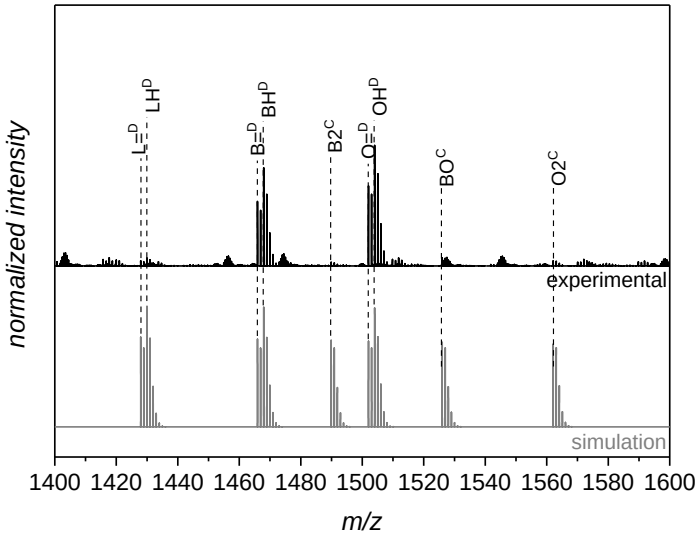

Figure S10. High resolution SEC-ESI mass spectra of p(BnMA) initiated by Irgacure 2959, synthesized at low laser energies (0.35 mJ/pulse, 100 Hz, 351 nm, black spectrum), and the associated isotopic pattern simulation (gray spectrum).

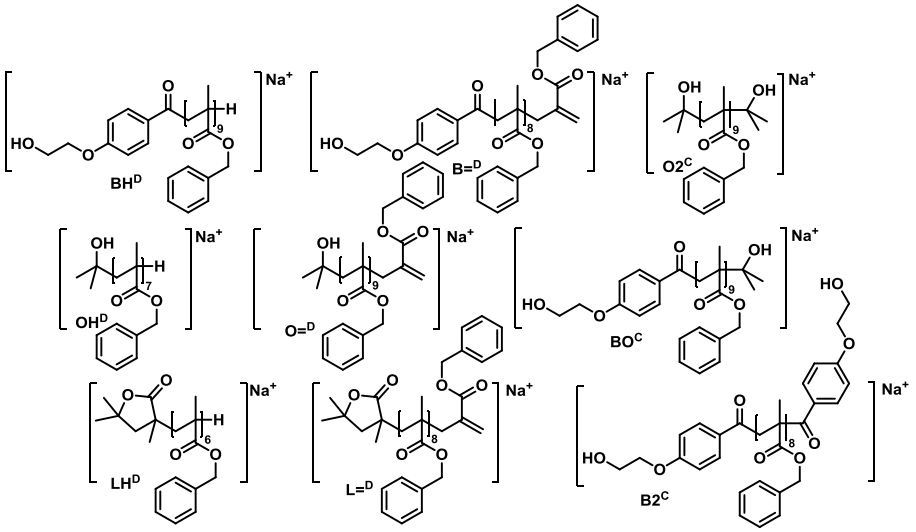

Scheme S9. Disproportionation and combination products of p(BnMA) initiated by Irgacure 2959, at low laser energies (0.35 mJ/pulse, 100 Hz, 351 nm), as detected by SEC-ESI-MS.

Table S9. Overview of the assigned signals of p(BnMA) synthesized at low laser energies (351 nm, 0.35 mJ/pulse, 100 Hz), as detected by SEC-ESI-MS with a resolution of 50000.

species	ionization	$(m/z)^{theo}$	$(m/z)^{exp}$	$\Delta(m/z)$
BH^{D}	Na^+	1773.8058	1773.8182	0.0124
B=^{D}	Na^+	1771.7901	1771.8005	0.0104
OH^{D}	Na^+	1843.8840	1843.8930	0.0090
O=^{D}	Na^+	1841.8684	1841.8857	0.0173
LH^{D}	Na^+	1735.8265	1735.8332	0.0067
L=^{D}	Na^+	1733.8109	1733.8199	0.0090
B2^{C}	Na^+	1761.7694	1761.7817	0.0123
O2^{C}	Na^+	1725.8422	1725.8110	0.0312
BO^{C}	Na^+	1831.8476	1831.8654	0.0176

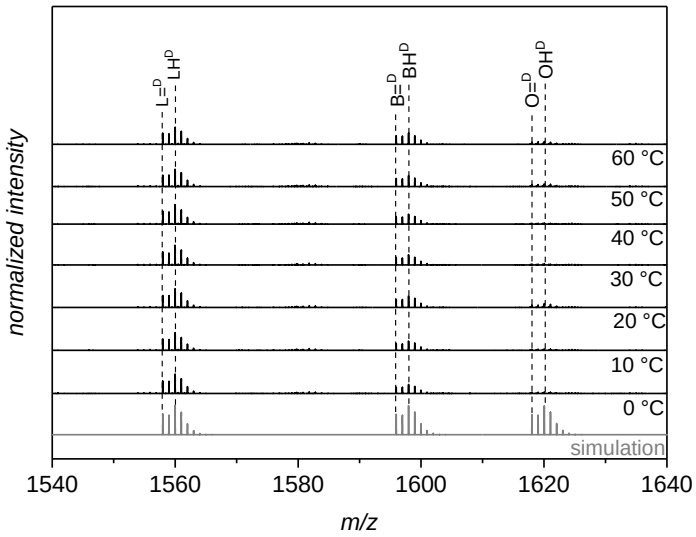

Figure S11. High resolution SEC-ESI mass spectra of p(BnMA) initiated by Irgacure 2959, synthesized at low laser energies (0.35 mJ/pulse, 100 Hz, 351 nm, black spectrum) at variable temperatures (0 °C – 60 °C) at a constant photon count and the associated isotopic pattern simulation (gray spectrum).

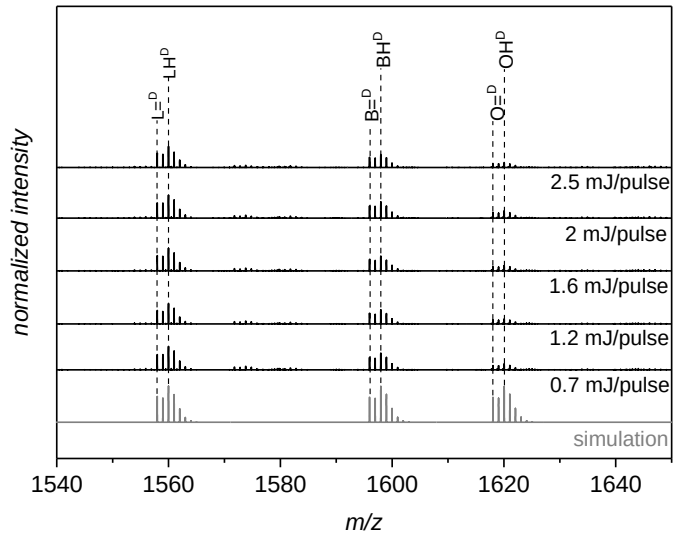

Figure S12. High resolution SEC-ESI mass spectra of p(BnMA) initiated by Irgacure 2959, synthesized at low laser energies (0.35 mJ/pulse, 100 Hz, 351 nm, black spectrum) at variable energies (0.7 mJ/pulse – 2.5 mJ/pulse) at a constant photon count and the associated isotopic pattern simulation (gray spectrum).

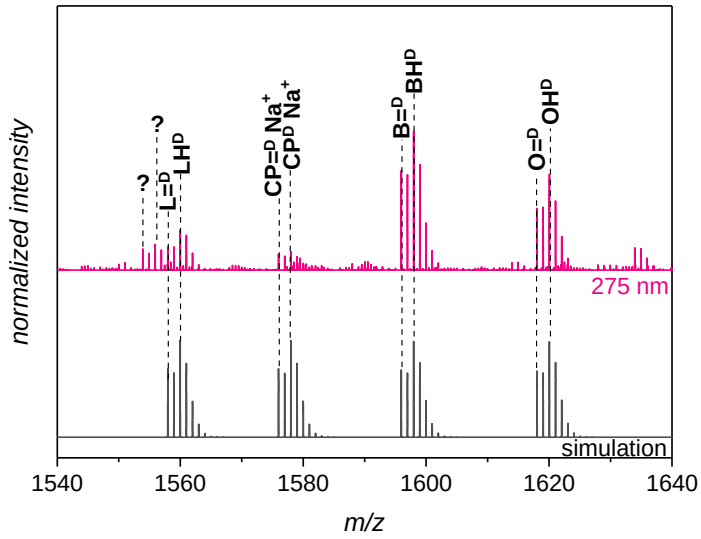

Figure S13. High resolution SEC-ESI mass spectra of p(*n*PMA) initiated by Irgacure 2959, synthesized at low laser energies (0.31 mJ/pulse, 100 Hz, 275 nm, pink spectrum) and the associated isotopic pattern simulation (gray spectrum).

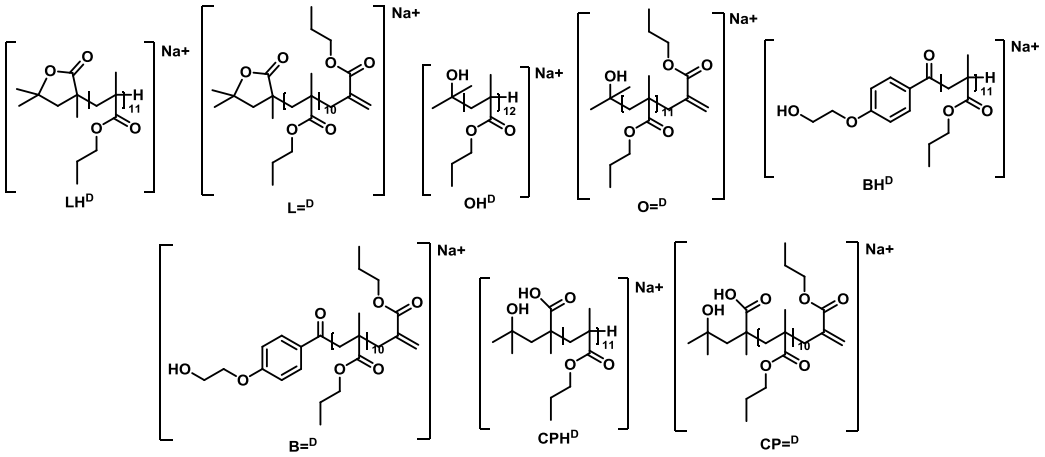

Scheme S10. Disproportionation and combination products of p(*n*PMA) initiated by Irgacure 2959, at low laser energies (0.31 mJ/pulse, 100 Hz, 275 nm, 18 °C), as detected by SEC-ESI-MS.

Table S10. Overview of the assigned signals of p(*n*PMA) synthesized at low laser energies (275 nm, 0.31 mJ/pulse, 100 Hz), as detected by SEC-ESI-MS with a resolution of 50000.

species	ionization	$(m/z)^{theo}$	$(m/z)^{exp}$	$\Delta(m/z)$
$\mathbf{BH}^{D}$	Na^+	1597.9732	1597.9718	0.0014
$\mathbf{B{=}}^{D}$	Na^+	1595.9576	1595.9593	0.0017
$\mathbf{OH}^{D}$	Na^+	1620.0515	1620.0460	0.0055
$\mathbf{O{=}}^{D}$	Na^+	1618.0358	1618.0379	0.0021
$\mathbf{LH}^{D}$	Na^+	1559.9940	1559.9948	0.0008
$\mathbf{L{=}}^{D}$	Na^+	1557.9783	1557.9806	0.0023
$\mathbf{CPH}^{D}$	Na^+	1578.0045	1578.0080	0.0035
$\mathbf{CP{=}}^{D}$	Na^+	1575.9889	1575.9926	0.0037

3.2 Ratio of Lactonization Product vs. the DP_n

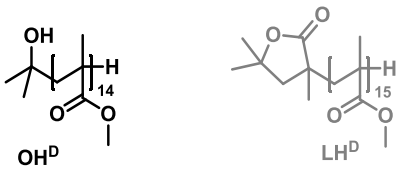

$$\chi^{\mathrm{LH^D}}(n) = \frac{\Delta h^{\mathrm{LH^D}}(n-1)}{\Delta h^{\mathrm{LH^D}}(n-1) + \Delta h^{\mathrm{OH^D}}(n)} \qquad \text{(eq. S2)}$$

$$\chi^{\mathrm{OH^D}}(n) = \frac{\Delta h^{\mathrm{OH^D}}(n)}{\Delta h^{\mathrm{LH^D}}(n-1) + \Delta h^{\mathrm{LH^D}}(n)} \qquad \text{(eq. S3)}$$

Table S11. Irradiation parameters and the amount of lactonization of p(*n*PMA) initiated by Irgacure 2959, given by the signal intensity ratio of LH^D.

Irradiation wavelength	**Target energy per pulse***[1]	**Number of pulses**	**Glass Transmission**	**Number of incident photons**	**Signal Intensity Ratio of LH^D**
λ / nm	**E / µJ**	**n_p**	**%**	**n_{ph} / µmol**	
275	314	90000	91.8	60	0.44
300	702	90000	37.7	60	0.68
320	440	90000	56.3	60	0.70
340	377	90000	61.9	60	0.73
360	331	90000	66.7	60	0.69

*[1]after deduction of the glass transmission

Table S12. Irradiation parameters and the amount of lactonization of the polymers initiated by Irgacure 2959, given by the signal intensity ratio of LH^D at 351 nm.

Polymers	Irradiation wavelength λ / nm	Target energy per pulse*[1] E / µJ	Number of pulses n_p	Glass Trans-mission %	Number of incident photons n_{ph} / µmol	Signal Intensity Ratio of LH^D
p(MMA)	351	350	90000	64.6	60	0.10
p(EMA)	351	350	90000	64.6	60	0.06
p(*n*PMA)	351	350	90000	64.6	60	0.78
p(*i*PMA)	351	350	90000	64.6	60	0.04
p(*n*BMA)	351	350	90000	64.6	60	0.06
p(*t*BMA)	351	350	90000	64.6	60	0.02
p(BnMA)	351	350	90000	64.6	60	0.83
p(DMAEMA)	351	350	90000	64.6	60	1.00

*[1]after deduction of the glass transmission

Table S13. Irradiation parameters and the amount of lactonization of p(*n*PMA) initiated by Irgacure 2959, given by the signal intensity ratio of LH^D at 351 nm.

Temperature °C	Target energy per pulse*[1] E / µJ	Number of pulses n_p	Glass Transmission %	Number of incident photons n_{ph} / µmol	Signal Intensity Ratio of LH^D
0	350	90000	64.6	60	0.93
10	350	90000	64.6	60	0.91
20	350	90000	64.6	60	0.82
30	350	90000	64.6	60	0.94
40	350	90000	64.6	60	0.94
50	350	90000	64.6	60	0.87
60	350	90000	64.6	60	0.85

*[1]after deduction of the glass transmission

Table S14. Irradiation parameters and the amount of lactonization of p(*n*PMA) initiated by Irgacure 2959, given by the signal intensity ratio of LH^D at 351 nm.

Energy*[1]	Number of pulses	Glass Transmission	Number of incident photons	Signal Intensity Ratio of LH^D
mJ/pulse	n_p	%	n_{ph} / µmol	
0.7	90000	64.6	119	0.80
1.2	90000	64.6	205	0.79
1.6	90000	64.6	273	0.81
2.0	90000	64.6	341	0.76
2.5	90000	64.6	426	0.80

*[1]after deduction of the glass transmission

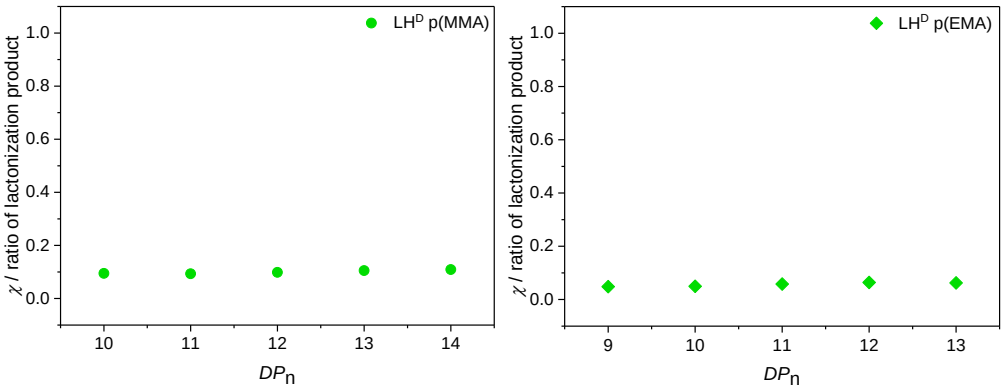

Figure S14. Plot of the lactonization product ratio of the peak height (**LH^D**) of p(MMA) and p(EMA) initiated by Irgacure 2959 vs. the DP_n at 351 nm.

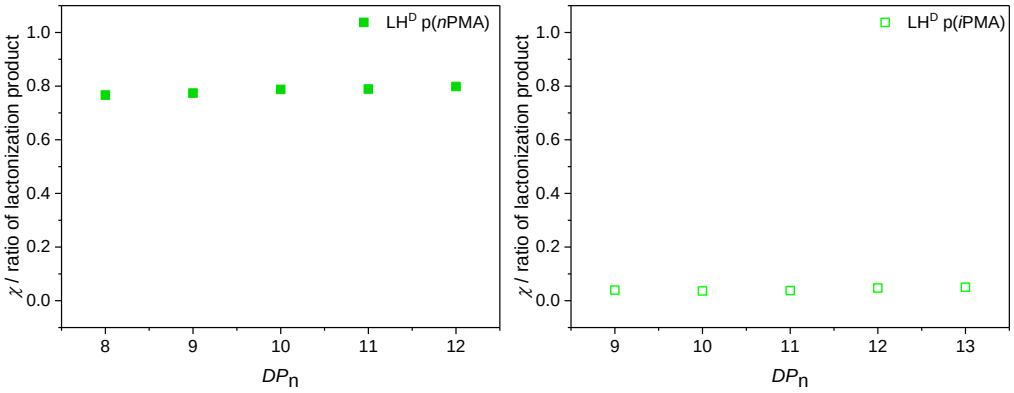

Figure S15. Plot of the lactonization product ratio of the peak height (**LH^D**) of p(*n*PMA) and p(*i*PMA) initiated by Irgacure 2959 *vs.* the DP_n at 351 nm.

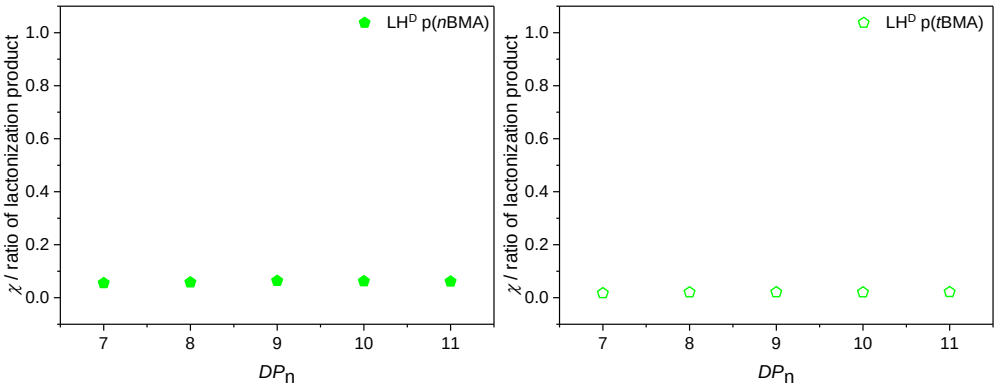

Figure S16. Plot of the lactonization product ratio of the peak height (**LH**^{D}) of p(*n*BMA) and p(*t*BMA) initiated by Irgacure 2959 *vs.* the DP_n at 351 nm.

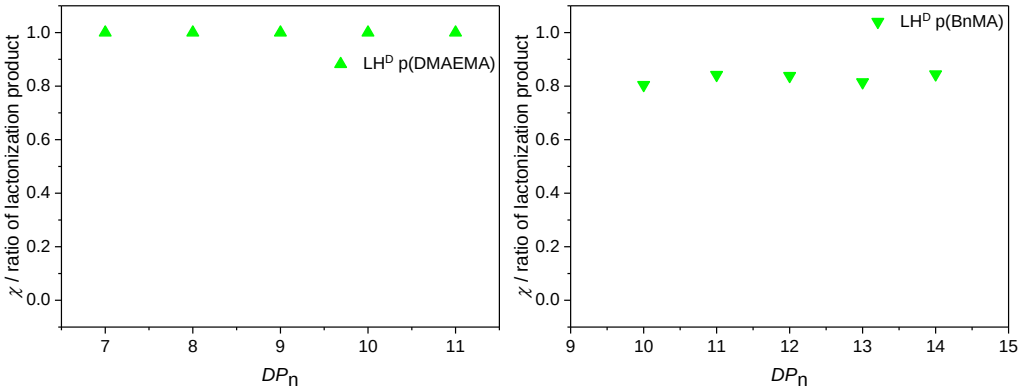

Figure S17. Plot of the lactonization product ratio of the peak height (**LH**^{D}) of p(BnMA) and p(DMAEMA) initiated by Irgacure 2959 *vs.* the DP_n at 351 nm.

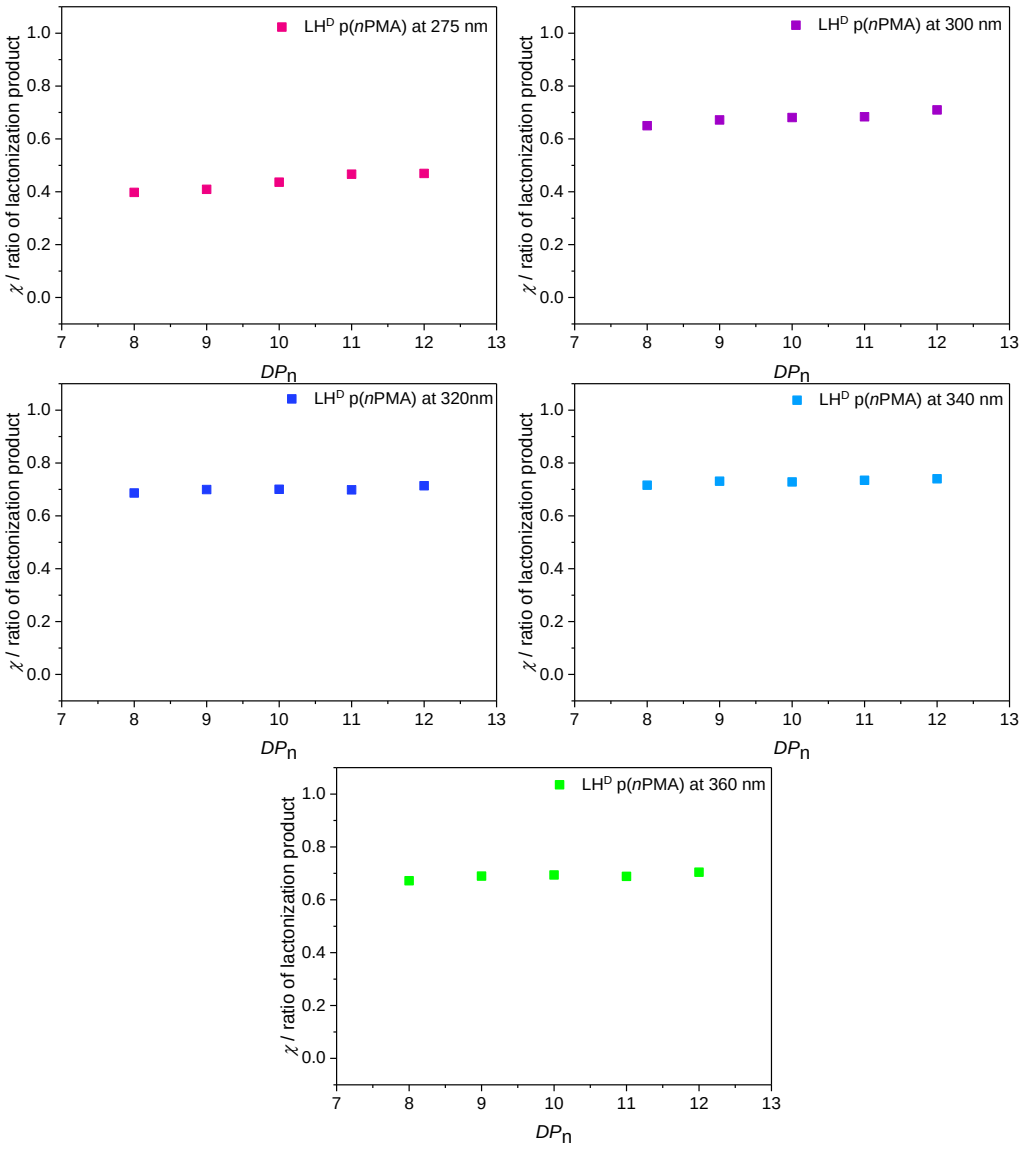

Figure S18. Plot of the lactonization product ratio of the peak height (**LH**^{D}) of p(*n*PMA) initiated by Irgacure 2959 *vs.* the DP_n between 275-360 nm.

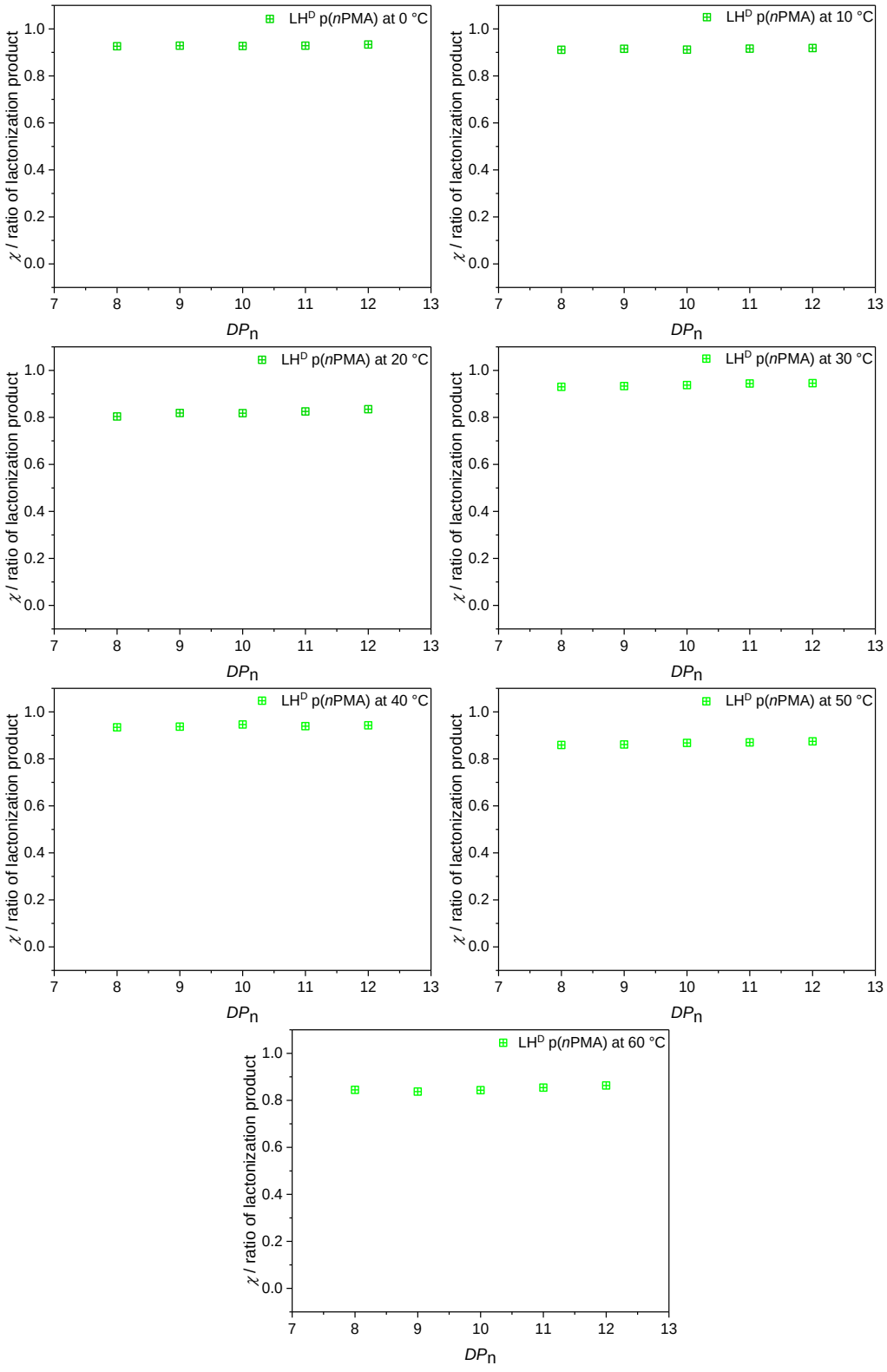

Figure S19. Plot of the lactonization product ratio of the peak height (**LH^{D}**) of p(*n*PMA) initiated by Irgacure 2959 (351 nm) *vs.* the DP_n between 0-60 °C.

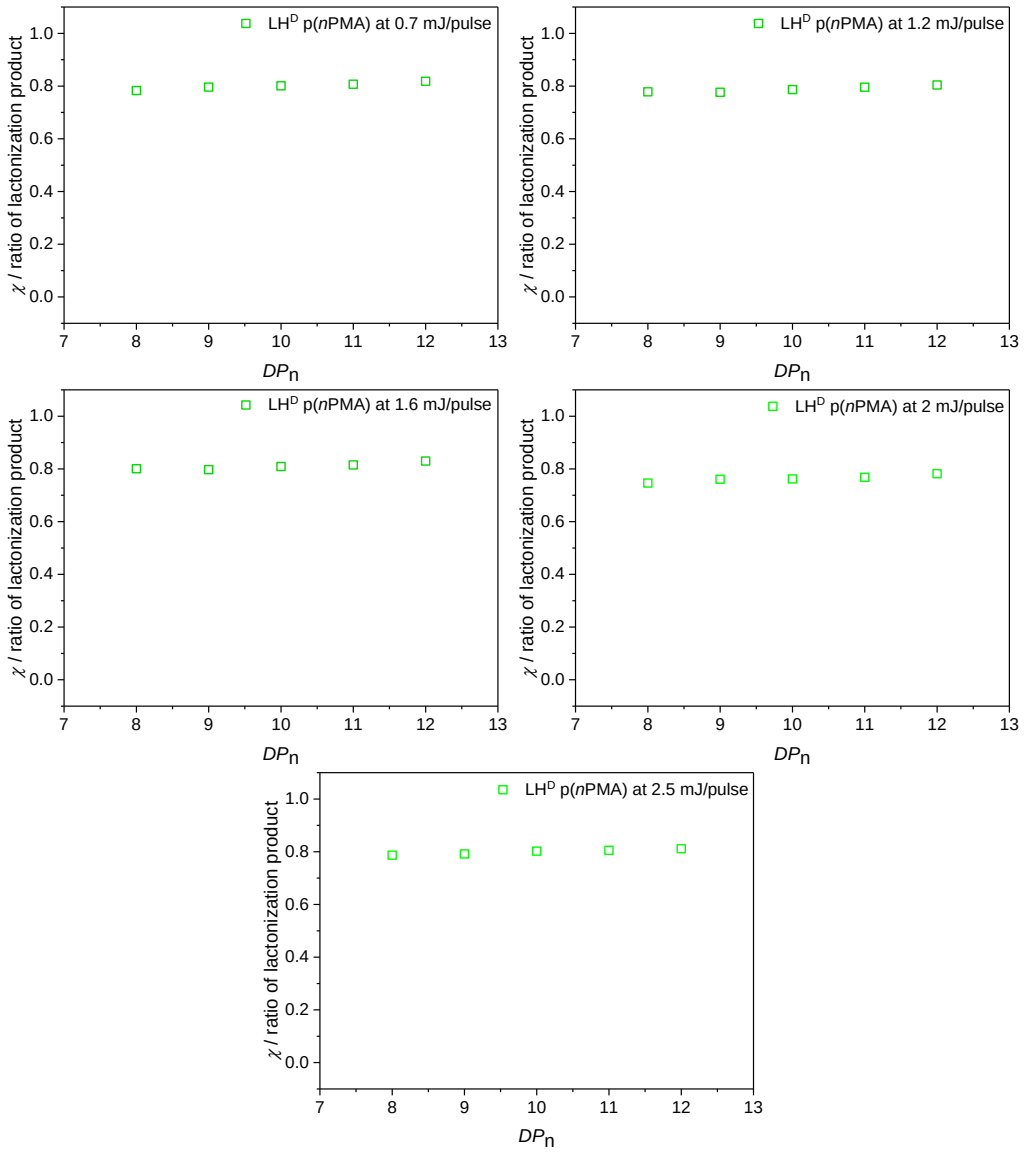

Figure S20. Plot of the lactonization product ratio of the peak height (**LH^{D}**) of p(*n*PMA) initiated by Irgacure 2959 (351 nm) *vs.* the DP_n between 0.7-2.5 mJ/pulse.

3.3 ^{13}C NMR spectra of p(nPMA) and p(nBMA)

Since the lactone is incorporated only as an end group into the polymer, 2D ^{13}C-^{13}C Incredible Natural Abundance DoublE QuAntum Transfer Experiments (INADEQUATE) to clearly determine the peak signals in the obtained ^{13}C NMR spectrum are not feasible, due to the insensitivity of such 2D experiment, as only 0.01% of the carbons are excited at natural abundance. Therefore, the ^{13}C NMR measurements served only as supporting information for the end group conversion, yielding the lactone species. Here, ^{13}C NMR measurements were conducted with two polymers, where one reveals the lactone species in the mass spectrum (p(*n*PMA)) and the other one does not (p(*n*BMA)). The obtained spectra are depicted in **Figure S21.**

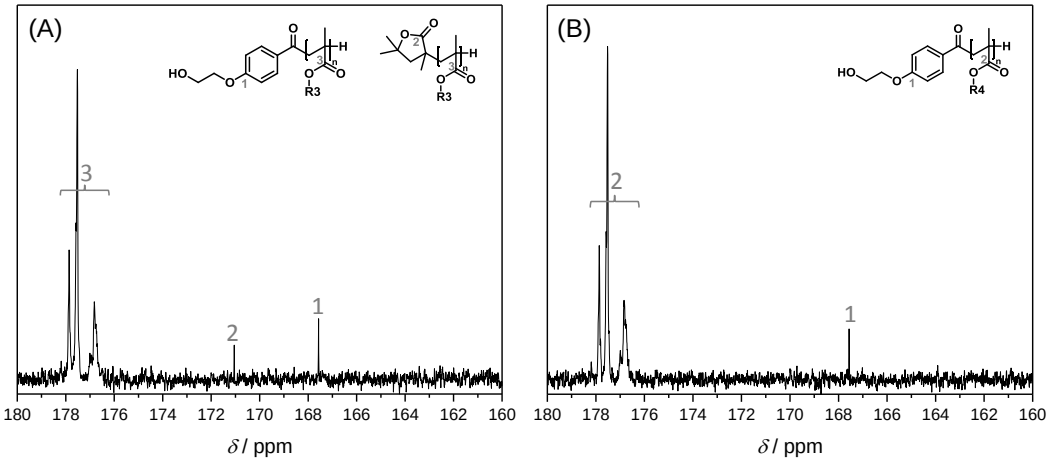

Figure S21. ^{13}C NMR spectra of p(*n*PMA) (A) and p(*n*BMA) (B) initiated by Irgacure 2959. For interests of simplicity only the C-O and C=O bond region is shown.

3.4 DFT Calculations

The reaction paths of spontaneous lactonization were calculated for the substituents propyl (**R3**) and butyl (**R4**) as described in **Scheme 1** of the main manuscript for *si* face and *re* face attack. From the open polymer end group conformation **OH_3** and **OH_4**, the transition states of lactonization ($TS_{ring\ closure}$) were located transforming to stable intermediates **I_3** and **I_4** after ring closure (see **Scheme S11**). After separation of the alcohol from the intermediate, the product of the reaction was located as a complex of alcohol (**R3-OH** and **R4-OH**) and the lactone (**LH_3** and **LH_4**), respectively. For time reasons, the transition state between the intermediates and the product lactone was not computed.

The S enantiotop polymer is 54 $kJ \cdot mol^{-1}$ more stable than the R enantiotop (see **Table S15**), which makes only the former experimentally accessible. Therefore the discussion of our DFT results concentrates on the reaction paths after *si* face attack (left side of **Figure S22**). The barriers of lactonization, i.e. the ring closure from open polymer end group **OH_3** and **OH_4** to the intermediates **I_3** and **I_4**, respectively, are similar for both substituents (~154 $kJ \cdot mol^{-1}$) and constitute the rate-limiting step. As presented in **Table S15**, the barriers of ring closure and the stability of the intermediates are similar for **R3** and **R4** substituents. The product complex, created after release of the alcohol (propanol, butanol) from the lactone (**LH_3**, **LH_4**), respectively, is thermodynamically stabilized for **R3** (-12 $kJ \cdot mol^{-1}$) whereas it is unstable for R4 (+2 $kJ \cdot mol^{-1}$).

For completeness, the lactonization intermediates and products of the unstable R enantiotop were also calculated. There exists a lower energy barrier (93.9 $kJ \cdot mol^{-1}$) with planar conformation inducing a possible modification of *si* face to *re* face polymer (right side of **Figure S22**). Both **R3** and **R4** product complexes are thermodynamically stable (~-45 $kJ \cdot mol^{-1}$ for *re* phase attack).

To sum up, our DFT calculations confirm the different reactivity of the **R3** and **R4** motifs from a thermodynamic point of view, because the S enantiotop can create a stable lactone after spontaneous ring closure and alcohol expellation.

Table S15 Relative Gibbs Free energies ΔG_{rel} in kJ·mol^{-1} for conformations after *si* face and *re* face attacks. Data are given for M06-2X/D3BJ/PCM/ aug-cc-pVDZ (aug-cc-pVTZ) method.[S2–S5,7]

***si* face attack (R3)**	**ΔG_{rel}** [a]
Polymer end group OH_3	0.0
$TS_{ring\ closure}$	153.7
	(157.3)
Intermediate I_3	22.8
	(27.1)
Complex of lactone LH_3 and propanol	-12.0
	(-13.5)
Transition State *si* ↔ *re* face attack (R3)	**ΔG_{rel}** [a]
TS_{planar} (*si* ↔ *re*)	93.9

***re* face attack (R3)**	**ΔG_{rel}** [a]	**ΔG_{rel}** [b]
Polymer end group OH_3	53.2	0.0
Intermediate I_3	36.9	-16.2
Complex of lactone LH_3 and propanol	8.0	-45.2

***si* face attack (R4)**	**ΔG_{rel}** [c]
Polymer end group OH_4	0.00
$TS_{ring\ closure}$	155.4
Intermediate I_4	29.4
Complex of lactone LH_4 and butanol	2.2

***re* face attack (R4)**	**ΔG_{rel}** [c]	**ΔG_{rel}** [d]
Polymer end group OH_4	53.5	0.0
Intermediate I_4	49.7	-3.8
Complex of lactone LH_4 and butanol	7.9	-45.6

[a] relative to the lowest energy *si* polymer end group OH_3.

[b] relative to the *re* face polymer end group OH_3.

[c] relative to the lowest energy *re* polymer end group OH_4.

[d] relative to the *re* face polymer end group OH_4.

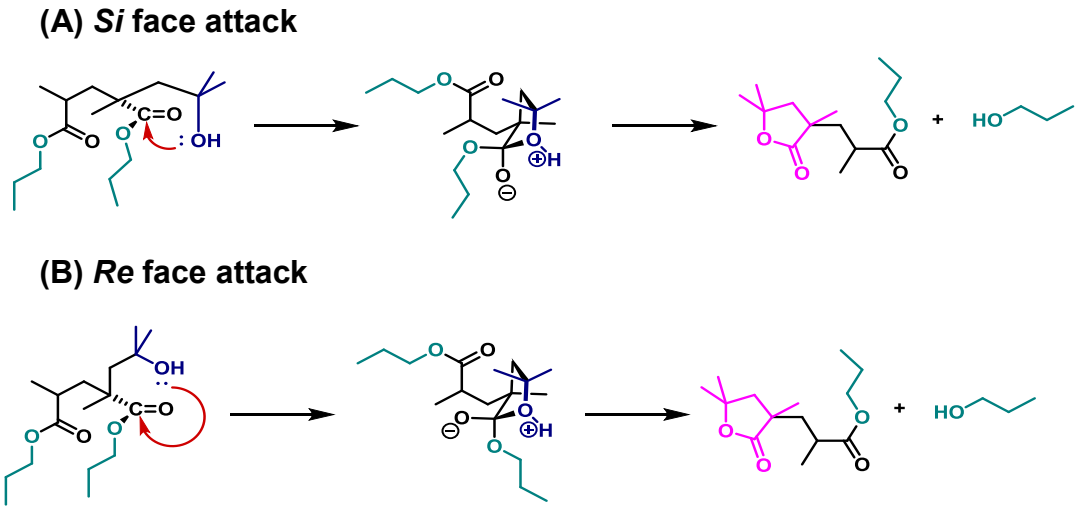

Scheme S11. Reaction paths of the propyl substituted molecule via *si* face attack (**A**) or *re* face attack (**B**).

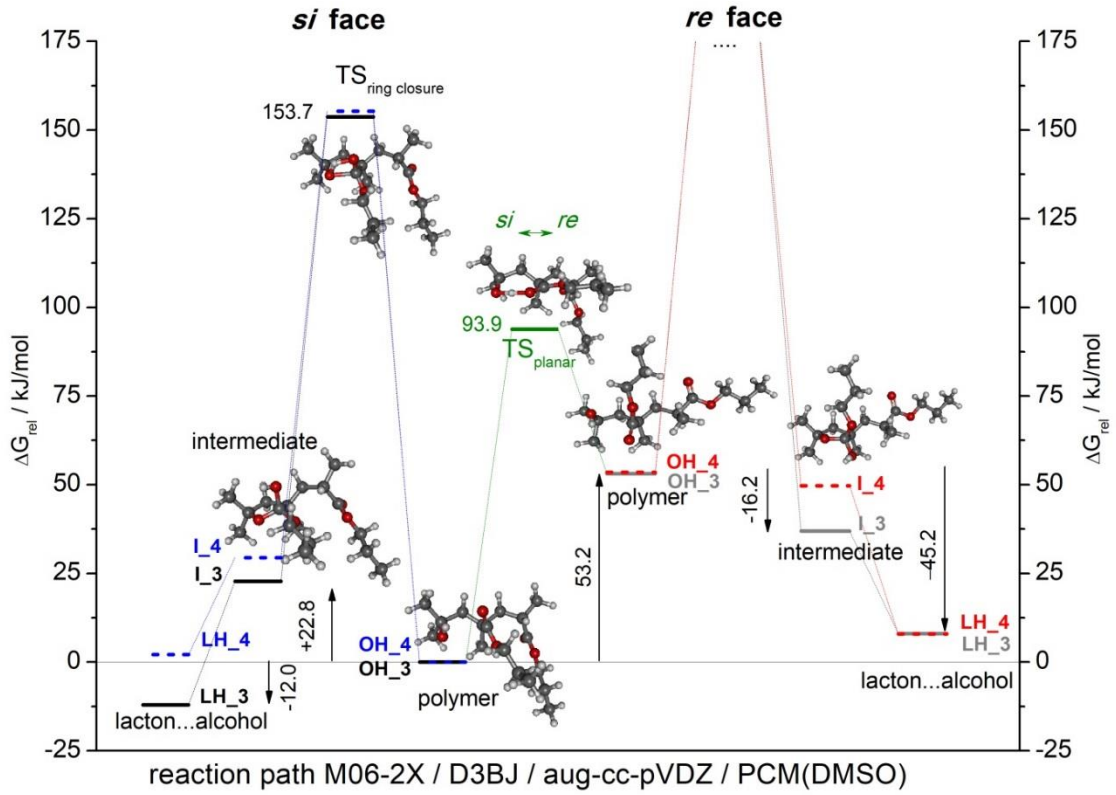

Figure S22. Lactonization reaction paths after *si* face (left) and *re* face (right) attacks. Gibbs free energies are given relative to the lowest-energy polymer, respectively.

4. References

(1) Fast, D. E.; Lauer, A.; Menzel, J. P.; Kelterer, A. M.; Gescheidt, G.; Barner-Kowollik, C. Wavelength-Dependent Photochemistry of Oxime Ester Photoinitiators. *Macromolecules* **2017**, *50*, 1815–1823.

(2) Zhao, Y.; Truhlar, D. G. The M06 Suite of Density Functionals for Main Group Thermochemistry, Thermochemical Kinetics, Noncovalent Interactions, Excited States, and Transition Elements: Two New Functionals and Systematic Testing of Four M06-Class Functionals and 12 Other Function. *Theor. Chem. Acc.* **2008**, *120*, 215–241.

(3) Grimme, S.; Antony, J.; Ehrlich, S.; Krieg, H. A Consistent and Accurate Ab Initio Parametrization of Density Functional Dispersion Correction (DFT-D) for the 94 Elements H-Pu. *J. Chem. Phys.* **2010**, *132*, 154104.

(4) Grimme, S.; Ehrlich, S.; Goerigk, L. Effect of the Damping Function in Dispersion Corrected Density Functional Theory. *J. Comput. Chem.* **2011**, *32*, 1456–1465.

(5) Dunning Jr, T. H. Gaussian Basis Sets for Use in Correlated Molecular Calculations. I. The Atoms Boron through Neon and Hydrogen. *J. Chem. Phys.* **1989**, *90*, 1007–1023.

(6) Kendall, R. A.; Dunning Jr, T. H.; Harrison, R. J. Electron Affinities of the First-Row Atoms Revisited. Systematic Basis Sets and Wave Functions. *J. Chem. Phys.* **1992**, *96*, 6796–6806.

(7) Mennucci, B.; Cammi, R.; Tomasi, J. Excited States and Solvatochromic Shifts within a Nonequilibrium Solvation Approach: A New Formulation of the Integral Equation Formalism Method at the Self-Consistent Field, Configuration Interaction, and Multiconfiguration Self-Consistent Field Level. *J. Chem. Phys.* **1998**, *109*, 2798–2807.

(8) Frisch, M. J.; Trucks, G. W.; Schlegel, H. B.; Scuseria, G. E.; Robb, M. A.; Cheeseman, J. R.; Scalmani, G.; Barone, V.; Mennucci, B.; Petersson, G. A.; et al. Gaussian 09, Revision D. 01. Gaussian, Inc., Wallingford CT **2009**.